J Physiol 587.8 (2009) pp 1715–1726

The Journal of Physiology

Functional maturation of the exocytotic machinery at gerbil hair cell ribbon synapses

Stuart L. Johnson[1], Christoph Franz[2], Marlies Knipper[2] and Walter Marcotti[1]

[1] *Department of Biomedical Science, University of Sheffield, Sheffield S10 2TN, UK*
[2] *Department of Otolaryngology, Tübingen Hearing Research Centre, Laboratory of Molecular Neurobiology and Cell Biology of the Inner Ear, University of Tübingen, D-72076 Tübingen, Germany*

Auditory afferent fibre activity in mammals relies on neurotransmission at hair cell ribbon synapses. Developmental changes in the Ca^{2+} sensitivity of the synaptic machinery allow inner hair cells (IHCs), the primary auditory receptors, to encode Ca^{2+} action potentials (APs) during pre-hearing stages and graded receptor potentials in adult animals. However, little is known about the time course of these changes or whether the kinetic properties of exocytosis differ as a function of IHC position along the immature cochlea. Furthermore, the role of afferent transmission in outer hair cells (OHCs) is not understood. Calcium currents and exocytosis (measured as membrane capacitance changes: ΔC_m) were measured with whole-cell recordings from immature gerbil hair cells using near-physiological conditions. The kinetics, vesicle pool depletion and Ca^{2+} coupling of exocytosis were similar in apical and basal immature IHCs. This could indicate that possible differences in AP activity along the immature cochlea do not require synaptic specialization. Neurotransmission in IHCs became mature from postnatal day 20 (P20), although changes in its Ca^{2+} dependence occurred at P9–P12 in basal and P12–P15 in apical cells. OHCs showed a smaller ΔC_m than IHCs that was reflected by fewer active zones in OHCs. Otoferlin, the proposed Ca^{2+} sensor in cochlear hair cells, was similarly distributed in both cell types despite the high-order exocytotic Ca^{2+} dependence in IHCs and the near-linear relation in OHCs. The results presented here provide a comprehensive study of the function and development of hair cell ribbon synapses.

(Received 5 January 2009; accepted after revision 17 February 2009; first published online 23 February 2009)
Corresponding author W. Marcotti: Department of Biomedical Science, University of Sheffield, Sheffield S10 2TN, UK. Email: w.marcotti@sheffield.ac.uk

Abbreviations APs, action potentials; ΔC_m, membrane capacitance changes; I_{Ca}, calcium current; IHCs, inner hair cells; OHCs, outer hair cells; P, postnatal day; RRP, readily releasable pool; SRP, secondarily releasable pool.

Sensory cells of hearing organs transduce sound into electrical responses. Two different sensory cells are present in the mammalian cochlea: inner hair cells (IHCs) and outer hair cells (OHCs). IHCs, the primary sensory receptors, respond to sound stimuli with sustained and graded receptor potentials. These responses are relayed to the brain with temporal precision (Fuchs, 2005) via the coordinated release of vesicles from IHC ribbon synapses onto type I spiral ganglion neurons (Glowatzki *et al.* 2008). Pre-hearing IHCs (≤P12 in most rodents) do not respond to sound but instead generate spontaneous Ca^{2+}-dependent action potentials (APs: Marcotti *et al.* 2003). Intracellular Ca^{2+} signalling associated with APs could regulate a variety of cellular responses involved in the cell's functional differentiation and/or maturation (Berridge *et al.* 2000; Spitzer *et al.* 2000), as proposed for the exocytotic machinery (Johnson *et al.* 2007). Neurotransmitter release from pre- and post-hearing IHCs is controlled by Ca^{2+} influx through L-type $Ca_V1.3$ Ca^{2+} channels (Platzer *et al.* 2000; Brandt *et al.* 2003), known to cluster at the cell's presynaptic site (Roberts *et al.* 1990; Tucker & Fettiplace, 1995). In contrast to IHCs, mature OHCs provide electromechanical amplification of the cochlear partition (Dallos, 1992) that is modulated by efferent fibres representing the majority of OHC synaptic connections (Guinan, 1996). However, during early postnatal development OHCs are transiently innervated by the same afferent fibres as IHCs (Pujol *et al.* 1998), express $Ca_V1.3$ Ca^{2+} channels (Michna *et al.* 2003) and show exocytotic responses (Beurg *et al.* 2008), indicating the possible presence of functional afferent synapses.

The synaptic machinery at mammalian hair cell ribbon synapses undergoes morphological (Sobkowicz *et al.* 1982) and biophysical (Beutner & Moser, 2001; Johnson *et al.*

DOI: 10.1113/jphysiol.2009.168542

2005) change with development in order to transmit the different physiological responses generated by pre- (spontaneous APs) and post-hearing (graded receptor potentials) cells. One example of functional maturation is the steeper exocytotic Ca^{2+} dependence of immature IHCs (Ca^{2+} cooperativity of about 4) compared to that observed in adult cells (mouse: Johnson *et al.* 2005; gerbils: Johnson *et al.* 2008). Although this Ca^{2+} dependence was similar in IHCs along the immature cochlea, tonotopic differences in the kinetics and Ca^{2+} sensitivity of exocytosis were present in adult gerbil IHCs (Johnson *et al.* 2008), which could enhance the signalling of receptor potentials in the low-frequency (phasic) and high-frequency (tonic) cells. Despite the investigations on gerbils and mice, there remains a shortage of information regarding the developmental time course for changes in the exocytotic Ca^{2+} sensitivity in IHCs as a function of their position along the mammalian cochlea. Moreover, very little is known about the kinetic properties and topographic organization of the synaptic machinery in immature hair cells. Therefore, the aims of the present study were to determine whether tonotopic differences in the kinetics of exocytosis and its Ca^{2+} coupling exist in immature IHCs and to study the maturation of the synaptic Ca^{2+} sensitivity. Finally, we investigated whether exocytosis in apical and basal immature OHCs differs from that of IHCs. The information presented provides the first biophysical and tonotopic correlation of hair cell ribbon synapse functional development before and at around the onset of hearing in mammals. All recordings, apart from those designed to investigate OHCs, were performed in near physiological conditions (body temperature and using 1.3 mM extracellular Ca^{2+}) to ensure a more realistic estimation of exocytosis at mammalian hair cell ribbon synapses.

Methods

The methods have been described fully before (Johnson *et al.* 2008) but important details are specified below.

Electrophysiology

Tissue preparation. Apical- and basal-coil IHCs ($n = 78$) from gerbils were studied in acutely dissected cochleae from postnatal day 5 (P5) to P16, where the day of birth is P0. This includes 13 IHCs (apical $n = 6$, P5–P6; basal: $n = 7$, P6–P7), used to determine the kinetics of exocytosis in Fig. 1*C* and *D*, that have been imported from Johnson *et al.* (2008) where they were only used to measure the Ca^{2+} dependence of vesicle release. The gerbil was preferred to the more commonly used mouse because of its extended low-frequency hearing range would emphasize any tonotopic differences (adult gerbil: ∼0.1–60 kHz; adult mouse: ∼2–100 kHz: Greenwood, 1990; Müller, 1996). A few P3 OHCs from gerbils ($n = 9$), C57B mice (apical-coil: $n = 6$) and Wistar rats (apical-coil: $n = 6$) were also investigated. All animals used for electrophysiology and some of those used for immunolabelling experiments were killed by cervical dislocation in accordance with UK Home Office regulations. The cochleae were dissected using the following extracellular solution (in mM): 135 NaCl, 5.8 KCl, 1.3 $CaCl_2$, 0.9 $MgCl_2$, 0.7 NaH_2PO_4, 5.6 D-glucose, 10 Hepes-NaOH, 2 sodium pyruvate. Amino acids and vitamins were added from concentrates (Eagle's minimal essential medium). The pH was adjusted to 7.5. The approximate position of apical and basal hair cells was measured as a fractional distance from the cochlear apex (for details see Johnson *et al.* 2008).

Patch clamp recording. All patch clamp recordings were performed near body temperature (34–37°C) using an Optopatch amplifier (Cairn Research Ltd, Faversham, UK). Patch pipettes were made from soda glass capillaries (2–3 MΩ) and coated with surf wax. The patch pipette filling solution contained (in mM): 106 caesium glutamate, 20 CsCl, 3 $MgCl_2$, 1 EGTA-CsOH, 5 Na_2ATP, 0.3 Na_2GTP, 5 Hepes-CsOH, 10 Na_2-phosphocreatine (pH 7.3). For some experiments BAPTA (0.1 mM, 0.6 mM, 1 mM) was used instead of 1 mM EGTA. Command protocols were applied and data acquired using pCLAMP software and a Digidata 1322A (Molecular Devices, Sunnyvale, CA, USA) and analysed with Origin (OriginLab Corp., Northampton, MA, USA). Synaptic vesicle exocytosis was measured as an increase in cell membrane capacitance (ΔC_m) that is generally interpreted as a sign of neurotransmitter release from presynaptic cells (Parsons *et al.* 1994; Moser & Beutner, 2000). Real-time ΔC_m was measured as previously described (Johnson *et al.* 2005). Briefly, a 4 kHz sine wave of 13 mV RMS was applied to cells from −81 mV and was interrupted for the duration of the voltage step. The capacitance signal from the Optopatch was amplified (×50), filtered at 250 Hz, sampled at 5 kHz and measured by averaging the C_m traces after the voltage step (around 200 ms) and subtracting from pre-pulse baseline. Experiments were performed during the superfusion of 30 mM TEA and 15 mM 4-AP to block most of the K^+ currents. Apamin (300 nM) and linopirdine (80–100 μM) were also added to the solution in order to block specifically I_{SK} and $I_{K,n}$, respectively. Calcium currents were corrected off-line for the linear leak conductance (g_{leak}) typically calculated between −81 mV and −71 mV (P5–P16 IHCs: 2.3 ± 0.1 nS, $n = 77$; P3 gerbil OHCs: 0.7 ± 0.1 nS, $n = 9$; P3 mouse OHCs: 1.0 ± 0.2 nS, $n = 6$; P3 rat OHCs: 1.0 ± 0.1 nS, $n = 6$). Membrane potentials were corrected for the voltage drop across the uncompensated series

resistance (P5–P16 IHCs: 5.8 ± 0.1 MΩ, $n = 78$; gerbil OHCs: 6.5 ± 0.6 MΩ, $n = 9$; mouse OHCs: 6.7 ± 0.5 MΩ, $n = 6$; rat OHCs: 7.3 ± 0.2 MΩ, $n = 6$) and for a liquid junction potential (−11 mV). IHC membrane capacitance (C_m) was 8.8 ± 0.2 pF (P5–P16: $n = 78$). OHC C_m was 6.2 ± 0.3 pF in gerbils ($n = 9$), 6.0 ± 0.2 pF in mice ($n = 6$) and 6.9 ± 0.8 pF in rats ($n = 6$).

Statistical comparisons of means were made by Student's two-tailed t-test or, for multiple comparisons, analysis of variance, one-way ANOVA followed by Tukey's test. Two-way ANOVA, followed by Bonferroni's test, was used to compare data sets from apical and basal IHCs. Means are quoted ± S.E.M. and $P < 0.05$ indicates statistical significance.

Immunocytochemistry

Immunostaining of gerbil IHCs was performed using otoferlin and CtBP2 antibodies as previously described (Schug *et al.* 2006; Johnson *et al.* 2008). Animals not processed in the UK were killed by CO_2 asphyxiation in accordance with the ethical guidelines approved by the University of Tübingen and the Tierschutzgesetz (Germany). Sections were viewed using an Olympus AX70 microscope equipped with epifluorescence illumination and motorization in the z-axis. Images were acquired using a CCD camera and the imaging software Cell^F (OSIS GmbH, Münster, Germany). For ribbon counts, cryo-sectioned cochleae were imaged over a distance of 8 μm with the complete coverage of the IHC nucleus and beyond in an image-stack along the z-axis (z-stack). Typically the z-stack consisted of 30 layers with a z-increment of 0.276 μm, for each layer one image per fluorochrome was acquired. To perform ribbon counts, z-stacks were three-dimensionally deconvoluted using Cell^F's RIDE module with the Nearest Neighbour algorithm and VoxelViewer. Figures 1*E* and 6*D* are representative single-layer images at the hair-cell nuclear plane. CtBP2 immunopositive ribbons and otoferlin staining were from apical and mid-basal immature IHCs from three gerbils (P4, P7 and P8). For each age tested between two and nine IHCs and one and five OHCs were analysed.

Results

Neurotransmitter release from pre-hearing gerbil IHCs

Tonotopic differences in the kinetic properties of synaptic vesicle release have recently been shown in adult gerbil IHCs (Johnson *et al.* 2008). Therefore, in this study we first investigated whether such kinetic differences were already present during pre-hearing stages (≤P12). A typical example of Ca^{2+} currents (I_{Ca}) and the corresponding ΔC_m recorded from immature apical- and basal-coil gerbil IHCs is shown in Fig. 1*A* and *B*. Responses were obtained using a 100 ms depolarizing voltage step (10 mV nominal increments) from −81 mV. The kinetics of neurotransmitter release in pre-hearing IHCs (P5–P7) was investigated by measuring ΔC_m near the peak I_{Ca} by varying the stimulus duration (from 2 ms to 1.5 s), which allowed the investigation of synaptic vesicle pool emptying (Fig. 1*C*). While relatively short stimuli revealed the number of vesicles in the readily releasable pool (RRP), longer steps induced the release of vesicles from a secondarily releasable pool (SRP) that is located further away from the Ca^{2+} channels (Moser & Beutner, 2000). Voltage steps of up to about 100 ms in apical and 50 ms in basal IHCs seemed to recruit mainly the RRP since ΔC_m responses could be approximated with a single exponential (Fig. 1*D*). The higher ΔC_m measured at 100 ms from some basal IHCs is likely to be caused by the earlier recruitment of the SRP. This was responsible for the apparently higher Ca^{2+} efficiency of exocytosis in early postnatal basal IHCs compared to age-matched apical cells (Johnson *et al.* 2008). The available RRP consisted of 400 and 510 synaptic vesicles in apical and basal IHCs, respectively, and had a similar initial release rate (Table 1). In order to determine whether the single ribbon synapse vesicle release rate varied as a function of IHC position along the cochlea, we performed ribbon counts on immature gerbil IHCs (Fig. 1*E*) using an antibody against the presynaptic ribbon component RIBEYE (CtBP2: Schmitz *et al.* 2000). The number of synaptic ribbons per IHC was similar in both regions of the cochlea (apical IHCs: 36.4 ± 1.2, $n = 15$; basal: 37.3 ± 0.8, $n = 16$) giving a release rate per ribbon of 355 and 360 vesicles s^{-1} in apical and basal IHCs, respectively, significantly different from that measured in basal adult cells only (Table 1: $P < 0.005$). The estimated number of readily releasable vesicles per ribbon was 10 in apical and 14 in basal immature IHCs, assuming that each active zone contributes equally to transmitter release. The size of the SRP (Fig. 1*C*) was also similar among immature IHCs and showed signs of saturation within the 1.5 s tested, not observed in adult IHCs (Johnson *et al.* 2008). An estimation of the SRP release rate was obtained by fitting the linear range of the data points (Fig. 1*C*, apical: 200–800 ms; basal: 100–600 ms). Linear regression indicated slopes of 216 vesicles s^{-1} (apical IHCs) and 214 vesicles s^{-1} (basal) per ribbon.

Figure 1*E* also shows the distribution of otoferlin, the proposed Ca^{2+} sensor of exocytosis in cochlear hair cells (Roux *et al.* 2006; Beurg *et al.* 2008). Otoferlin was detected throughout the cytoplasm of immature IHCs with a higher expression level at the active zones (in the same region as RIBEYE) and usually below the cell's cuticular plate, where synaptic vesicle internalization is likely to occur (Griesinger *et al.* 2005). Although some variability in staining intensity was observed among preparations, we

could not detect any consistent difference in the expression of otoferlin between apical and basal IHCs (judged from the qualitative observations of more than 50 sections). This labelling pattern was also similar to that previously described for IHCs of adult gerbils (Johnson *et al.* 2008), rats and mice (Schug *et al.* 2006).

Vesicle pool depletion in apical and basal immature IHCs

Immature IHCs are known to produce trains of spontaneous Ca^{2+} action potentials (Marcotti *et al.* 2003), the frequency of which could increase along the length of the cochlea up to a maximum of just below 10 Hz in basal cells (Johnson & Marcotti, 2008). The ability of these IHCs to maintain bouts of vesicle release was investigated by using repetitive stimuli of different durations (designed to release predominantly RRP or SRP: Fig. 2*A* and *B*, respectively). These experiments were carried out in order to determine whether vesicle pool refilling could become rate limiting for vesicle release in these cells. Following repeated 50 ms steps (stimulus frequency about 7 Hz), which induce RRP exocytosis in IHCs and correspond to about the width of an action potential (Marcotti *et al.* 2003), the cumulative ΔC_m showed a near linear increase (Fig. 2*C*). This indicates that both apical and basal IHCs were able to replenish their RRP following

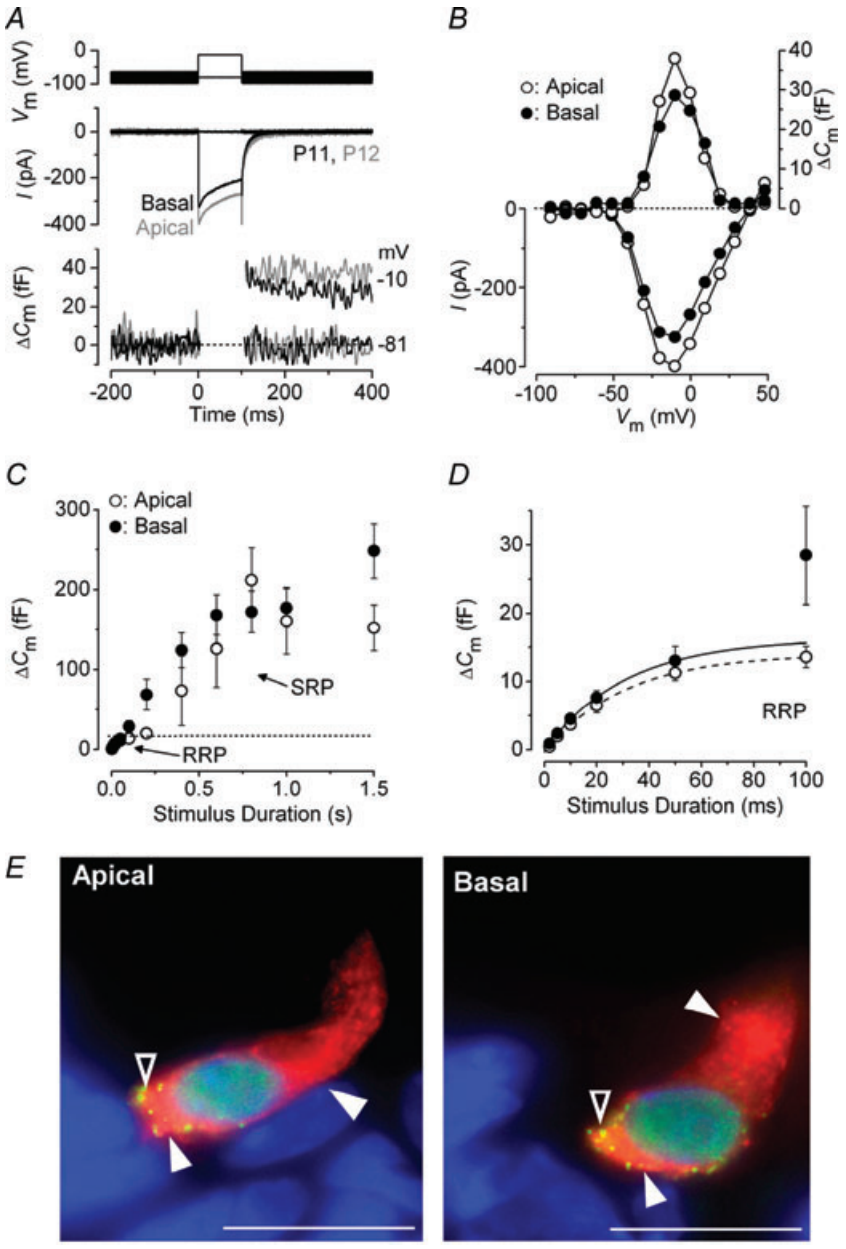

Figure 1. Neurotransmitter release in immature IHCs
A, I_{Ca} (middle panel) and ΔC_m (bottom panel) responses recorded from apical (grey traces) and basal (black traces) IHCs of the gerbil cochlea at around the onset of hearing. Recordings were obtained in response to 100 ms voltage steps from the holding potential of −81 mV to near −10 mV. The voltage protocol is shown in the top panel. *B*, current–voltage (*I–V*, bottom panel) and capacitance–voltage (ΔC_m–*V*, top panel) curves from the IHCs shown in *A*. Recordings were obtained in response to 10 mV depolarizing voltage steps (100 ms) from −81 mV. *C*, average ΔC_m responses from six apical (P5–P6) and ten basal (P6–P7) IHCs. Recordings were obtained by applying voltage steps from 2 ms to 1.5 s (to around −11 mV) in order to elicit both the RRP and SRP. *D*, expanded version of the first 100 ms shown in *C* where data up to 50 ms have been approximated with single exponential functions (apical: maximum $\Delta C_m = 14.1 \pm 2.7$ fF, $\tau = 30.7 \pm 12.5$ ms; basal: maximum $\Delta C_m = 16.3 \pm 4.2$ fF, $\tau = 30.9 \pm 17.2$ ms). The RRP consisted of 400 ± 45 (apical: $n = 6$, P5–P6) and 510 ± 96 (basal: $n = 10$, P6–P7) synaptic vesicles using a conversion factor of 37 aF per vesicle (Lenzi *et al.* 1999). Unless otherwise stated, in this and the following figures recordings were obtained at body temperature and using physiological 1.3 mM extracellular Ca^{2+}. *E*, immunolocalization of synaptic ribbons (CtBP2: green dot-like pattern indicated by open arrowheads) and otoferlin (red: filled arrowheads) in apical and basal P4 IHCs. Nuclei were stained with DAPI (blue). Scale bars represent: 10 μm.

Table 1. Synaptic ribbon properties in gerbil hair cells

	Immature OHCs (3rd row)		Immature IHCs		Adult IHCs	
	Apical	Basal	Apical	Basal	Apical	Basal
Ca^{2+} dependence of exocytosis (power *N*)	0.7	1.1	3.6	3.9	2.2	1.0
Ribbon no.	18	22	36	37	21	22
Vesicles in the total RRP	135	143	400	510	534	619
RRP vesicles per ribbon	8	7	11	14	26	28
RRP release rate (vesicles s^{-1})	—	—	12 911	13 425	10 449	14 883
RRP release rate per ribbon (vesicles s^{-1})	—	—	355	360	507	664
SRP release rate (vesicles s^{-1})	—	—	8208	7933	2335	1695
SRP release rate per ribbon (vesicles s^{-1})	—	—	216	214	111	77
SRP depletion time constant (s)	—	—	8.6	4.8	12.0	21.3

All numbers reported are mean values. S.E.M. and cell numbers for immature data are given in Results. Adult values are obtained or calculated from Johnson *et al.* 2008. For immature OHCs, recording were only performed from the outer row (3rd row) of cells. The ribbon number and RRP vesicles per ribbon in immature OHCs are based on the estimation of two ribbons per active zone (see Results). OHC exocytotic kinetics were not measured. We did not observe any RRP depletion in both immature and adult IHCs using 50 ms voltage steps (at about 7 Hz).

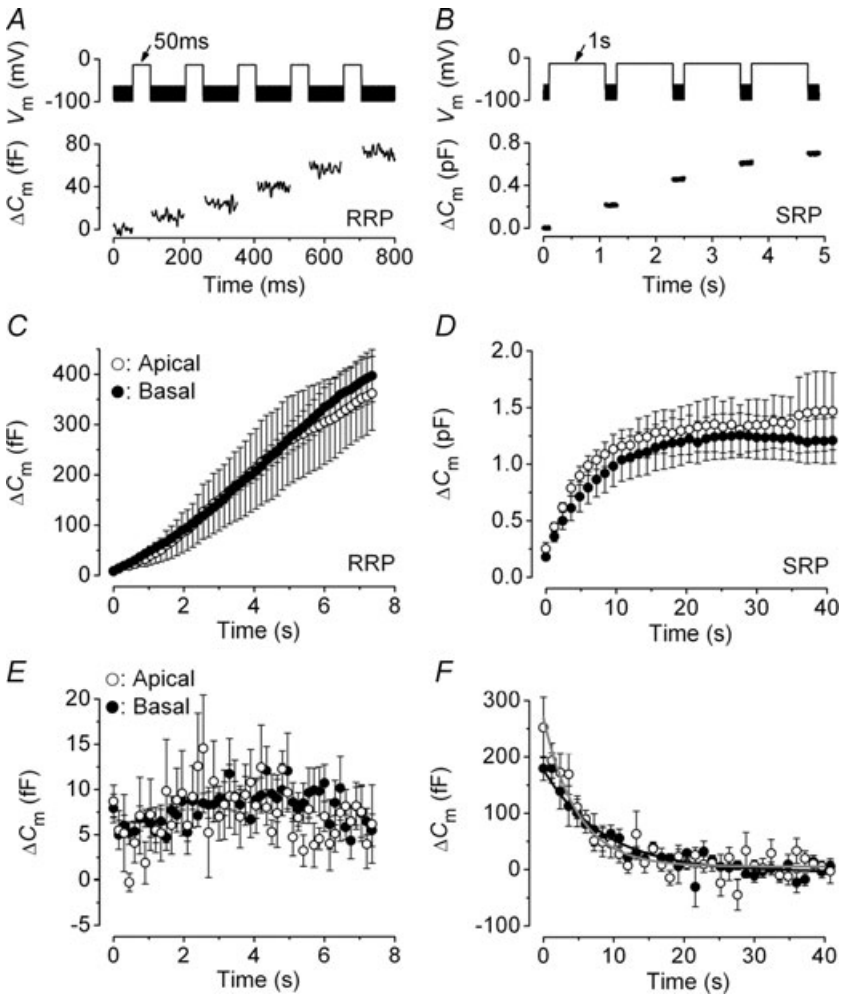

Figure 2. Depletion of synaptic vesicle pools in immature IHCs
A and *B*, ΔC_m responses from basal-coil IHCs (P7) elicited using repetitive voltage steps to near −11 mV. The duration of the voltage step was selected in order to elicit the RRP (*A*: 50 ms) or the SRP (*B*: 1 s), with an interstep-interval of 100 ms or 200 ms, respectively. For clarity, only the first few steps are shown. The voltage protocol used is shown above the traces. *C* and *D*, average cumulative ΔC_m values elicited using 50 (RRP) and 35 (SRP) steps from P7–P10 apical (RRP: $n = 6$; SRP: $n = 7$) and basal (RRP: $n = 11$; SRP: $n = 10$) IHCs, respectively. *E* and *F*, individual ΔC_m values measured following each voltage step from panels *C* and *D*, respectively, in both apical and basal IHCs. Fits in *F* are according to a first-order exponential equation.

each step. The overall individual ΔC_m (Fig. 2*E*) was found to be similar between apical (7.2 ± 0.4 fF, $n = 6$) and basal (7.9 ± 0.3 fF, $n = 11$) immature IHCs. Following repetitive long-lasting (1 s) voltage steps (200 ms interstep intervals), the cumulative ΔC_m showed saturation of SRP release in both apical and basal IHCs (Fig. 2*D*), which was also evident from the individual ΔC_m (Fig. 2*F*). The depletion time constant was 8.6 s and 4.8 s in apical and basal IHCs, respectively. The absence of the initial potentiation of SRP exocytosis in pre-hearing IHCs, which was found in adult cells (Johnson *et al.* 2008), is likely to be due to the recruitment of the entire pool in response to the first step. Potentiation was evident by P16 in IHCs from both cochlear regions (data not shown). Although long-lasting (1 s) protocols are of less physiological relevance for immature spiking IHCs, it allowed us to compare the properties of SRP refilling to adult IHCs (Table 1).

Developmental changes in the Ca^{2+} sensitivity of exocytosis

The Ca^{2+} sensitivity of neurotransmitter release in gerbil IHCs changes between immature and adult stages (Johnson *et al.* 2008). However, the time course of this transition is still unknown. In order to present a more comprehensive picture of the development in exocytotic Ca^{2+} sensitivity, values from immature (apical: P5–P6; basal: P6–P7) and adult (>P20) IHCs used in Figs 3 and 4*C* (see below) are derived from cells included in Johnson *et al.* (2008). Figure 3*A* shows the average size of I_{Ca}, measured near the peak of the *I–V* curves (see Fig. 1*B*), as a function of postnatal age and IHC position in the cochlea. In order to obtain a better representation of the change in I_{Ca} during the main stages of IHC functional development, values were pooled into three age groups (Fig. 3*A* and *B*: immature, intermediate and adult). Apical and basal IHCs showed a significant decrease in the size of I_{Ca} with development (Fig. 3*B*, overall $P < 0.0001$). However, during the same period, no significant difference in ΔC_m was found between IHCs from both cochlear regions (Fig. 3*C* and *D*). The difference between the development of I_{Ca} and ΔC_m was indicative of an increased Ca^{2+} efficiency of exocytosis (defined as $\Delta C_m/I_{Ca}$) with maturation as shown in Fig. 3*E* and *F* (overall $P < 0.0001$ for both apical and basal IHCs).

The Ca^{2+} dependence of synaptic vesicle release in immature IHCs (Fig. 4), defined as the change in ΔC_m as a function of I_{Ca}, was measured using the synaptic transfer curve (Augustine *et al.* 1985; Johnson *et al.* 2008). This was obtained by plotting ΔC_m values against the

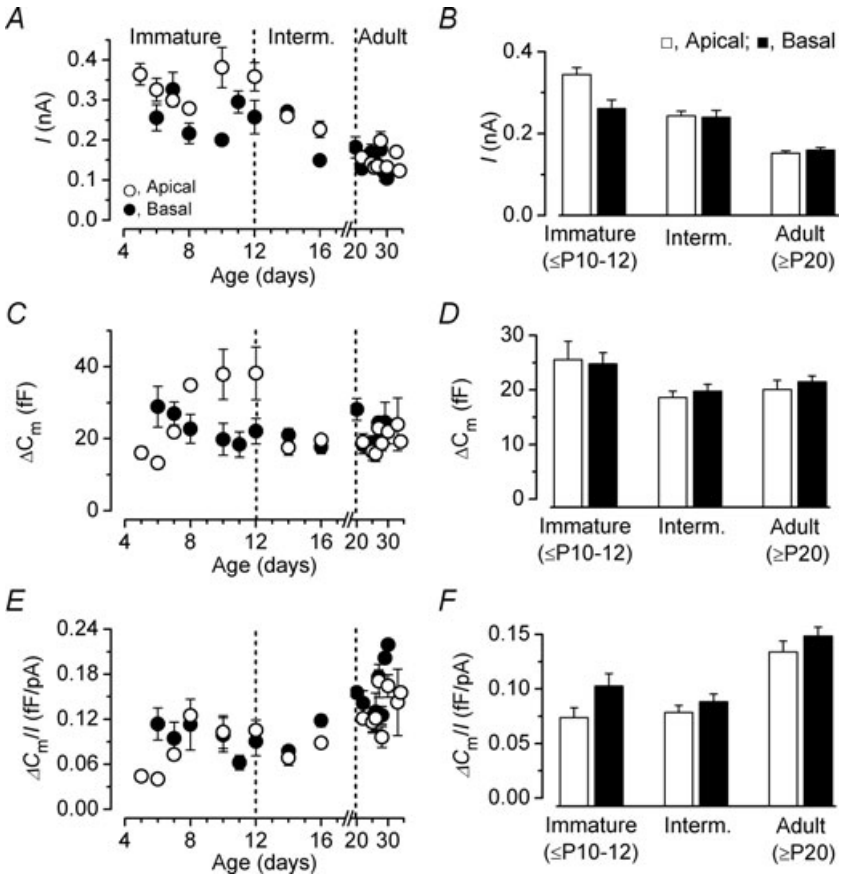

Figure 3. Changes in Ca^{2+} efficiency of exocytosis in developing gerbil IHCs
A, size of I_{Ca} from near the peak of individual *I–V* curves (see Fig. 1*B*) as function of postnatal day. *B*, average size of I_{Ca} grouped into the three main stages of cochlear development shown in panel *A*: Immature, Intermediate and Adult. One-way ANOVA with Tukey's *post hoc* test indicates $P < 0.001$ for all combinations apart from immature *vs*. intermediate basal cells, which was not significant. *C* and *D*, development of ΔC_m. *E* and *F*, development of the Ca^{2+} efficiency of exocytosis. In panel *F* the *post hoc* test indicates $P < 0.01$ or higher apart from immature *vs*. intermediate cells, which was not significant. Numbers of cells in panels *A–F*: apical (P5–P34): 2, 7, 1, 1, 4, 4, 5, 5, 6, 4, 3, 2, 3, 5, 6, 1; basal (P6–P30): 3, 6, 3, 4, 4, 4, 5, 5, 2, 4, 5, 3, 4, 3, 2, 1.

corresponding I_{Ca} between −71 mV and −11 mV (see Fig. 1*B*). Data were approximated using a power function:

$$\Delta C_m = cI_{Ca}^N \quad (1)$$

where c is a scaling coefficient and the power is N. For this comparison the peak I_{Ca} was used, instead of its time integral, to avoid possible errors due to the presence of the residual unblocked K^+ current as previously described (Johnson *et al.* 2005, 2008). Figure 4*A* and *B* shows averaged transfer functions from apical and basal IHCs that have been grouped into pre- and post-hearing stages (see Fig. 4*C* for a better overview of the age range selected). For basal IHCs, an additional group showing the transfer function at the onset of hearing is included. A detailed representation of the developmental change in the exocytotic Ca^{2+} dependence as a function of days after birth is shown in Fig. 4*C*. Fits to the data in Fig. 4*C* are according to a sigmoidal logistic growth curve:

$$N = N_{min} + \frac{(N_{max} - N_{min})}{1 + \exp(-k(t - t_{half}))} \quad (2)$$

where k is a slope factor, t_{half} is the age where N is halfway between the maximal (N_{max}) and minimal (N_{min}) power. The fits gave values for t_{half} and k of P13.7 and 2.6 day^{-1} in apical and P10.6 and 2.5 day^{-1} in basal IHCs. The linearization in Ca^{2+} dependence occurred very rapidly from around the beginning of the second postnatal week in basal IHCs and was complete by the onset of hearing at P12. Contrary to basal IHCs, the high Ca^{2+} dependence of exocytosis in apical cells was only slightly reduced from just after the onset of hearing.

Functional coupling between Ca^{2+} channels and the RRP in pre-hearing IHCs

The developmental changes in the exocytotic Ca^{2+} dependence in apical and basal IHCs (Fig. 4) could arise from variations in the coupling between Ca^{2+} influx and the release-ready pool (RRP) of vesicles. In adult gerbil IHCs Ca^{2+} channels are localized within a nanodomain of the synaptic machinery (Johnson *et al.* 2008). Therefore, we investigated whether the higher exocytotic Ca^{2+} dependence in pre-hearing IHCs resulted from a weaker (microdomain) coupling to Ca^{2+} channels. The distance between Ca^{2+} channels and presynaptic release sites was estimated by measuring exocytosis in both apical and basal IHCs whilst using either intracellular EGTA (1 mM) or different concentrations of the faster Ca^{2+} chelator BAPTA (Fig. 5*A–D*), which is capable of buffering Ca^{2+} elevations closer to their source (Neher, 1998). For these experiments we used a similar voltage protocol to that described in Fig. 1*D* (voltage steps between 5 ms and 100 ms) in order to recruit mainly the RRP. The release of the RRP was unaffected when pre-hearing IHCs were buffered with 0.1 and 0.6 mM BAPTA (Fig. 5*E*). However, 1 mM BAPTA almost completely blocked RRP exocytosis in both cochlear regions (apical: $P < 0.01$; basal: $P < 0.001$; relative to recordings in 1 mM EGTA). This indicates a similar distance between Ca^{2+} channels and release sites in immature IHCs positioned at each end of the cochlea (in the range of 40 nm: Naraghi & Neher, 1997).

Neurotransmitter release in immature OHCs

A recent investigation has shown that pre-hearing OHCs from *Otoferlin* (*Otof*) control mice exhibit robust neurotransmitter release (Beurg *et al.* 2008). This led us to look for possible position-dependent differences in OHC exocytosis using immature P3 gerbils. Initially, we performed experiments using physiological 1.3 mM

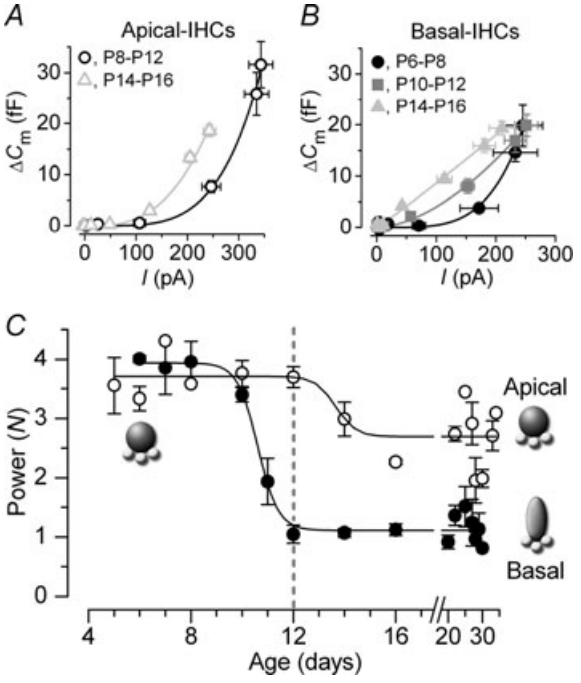

Figure 4. Changes in Ca^{2+} dependence of exocytosis in gerbil IHCs
A and *B*, examples of synaptic transfer functions obtained by plotting average ΔC_m against the corresponding I_{Ca} from *I–V* and ΔC_m–*V* curves (as in Fig. 1*B*: voltage range –71 mV to −11 mV) of apical and basal IHCs, respectively. Data were grouped into age ranges at around the onset of hearing at P12. Fits are according to eqn (1). Values of *N* were: apical 4.3 (P8–P12, $n = 12$) and 3.0 (P14–P16, $n = 10$); basal 4.2 (P6–P8, $n = 4$), 1.7 (P10–P12, $n = 12$) and 1.1 (P14–P16, $n = 10$). *C*, developmental changes in *N* from both apical and basal IHCs as a function of days. Data points were obtained by averaging *N* values from fits to synaptic transfer functions of single cells using eqn (1). Note that basal IHCs start to mature a few days earlier than apical IHCs. The fits to the averaged data points are according to eqn (2). Numbers of cells: apical (P5–P34): 2, 7, 1, 1, 4, 4, 5, 5, 2, 1, 2, 3, 5, 2, 1; basal (P6–P30): 3, 6, 3, 4, 4, 4, 5, 5, 2, 2, 3, 2, 2, 2, 1.

extracellular Ca^{2+}. Under these experimental conditions ΔC_m was very small and could not be accurately measured. Therefore, I_{Ca} and ΔC_m were recorded from OHCs in 5 mM extracellular Ca^{2+} (Fig. 6*A*). Despite this, ΔC_m was still relatively small and in order to obtain reliable measurements, especially for small I_{Ca}, traces recorded from all OHCs within each cochlear region were averaged. Higher Ca^{2+} concentrations could not be tested because they rapidly cause the preparation to deteriorate when working at body temperature (Johnson *et al.* 2005). The size of both the peak I_{Ca} (apical OHCs: -113 ± 18 pA, $n = 4$; basal OHCs: -83 ± 15 pA, $n = 4$) and maximal ΔC_m (apical: 5.0 fF; basal: 5.3 fF), elicited using 100 ms steps, did not vary significantly along the cochlea (Fig. 6*B*). This indicates that the Ca^{2+} efficiency of exocytosis was similar between apical and basal OHCs. Although the size of I_{Ca} was comparable to that recently reported in *Otof* control OHCs (Beurg *et al.* 2008), ΔC_m was surprisingly about 9 times smaller. At first we thought that this could be down to the different animal species used for the two studies (control *Otof* mice and gerbils), so we performed additional experiments in P3 OHCs from normal C57B mice and Wistar rats. Despite their larger peak I_{Ca} (mouse: -190 ± 19 pA, $n = 6$; rat: -151 ± 26 pA, $n = 6$), the maximal size of ΔC_m remained relatively small (mouse: 7.0 ± 0.7 fF; rat: 7.8 ± 1.0 fF) and similar to that of gerbil OHCs (Fig. 6*C*). For the results obtained from gerbil OHCs, synaptic transfer functions (see above) were used to measure the Ca^{2+} dependence of exocytosis (Fig. 6*C*). The power values were 0.7 ± 0.1 ($n = 4$) in apical and 1.1 ± 0.1 ($n = 4$) in basal OHCs (Fig. 6*C*), indicating a near linear relation between Ca^{2+} entry and exocytosis as previously described (mouse *Otof* control OHCs: Beurg *et al.* 2008). Although we did not measure directly the release kinetics of the RRP (the very small ΔC_m in OHCs limited the accuracy of recording responses to very short stimuli) we estimated its overall size using a 100 ms voltage step. This is likely to be a reliable measure since the same stimulus almost completely isolated the RRP in mouse OHCs (Beurg *et al.* 2008). Using this method, the RRP in gerbil OHCs consisted of about 135 vesicles and 143 vesicles in apical and basal cells, respectively. In agreement with the findings in IHCs (Fig. 1*E*), the number of CtBP2 positive dot-like spots per OHC (i.e. active zones) was similar along the cochlea (Fig. 6*D*: 3rd row OHCs: apical 9; basal 11). The size of these spots were usually larger than that seen in IHCs (see also Beurg *et al.* 2008) most likely reflecting multiple synaptic ribbons at OHC active zones (Shnerson *et al.* 1982). Considering that on average two synaptic ribbons could be present at each active zone, the number of vesicles per ribbon in the RRP in immature OHCs is likely to be about eight. The intensity and distribution of otoferlin labelling was similar among OHCs (Fig. 6*D*).

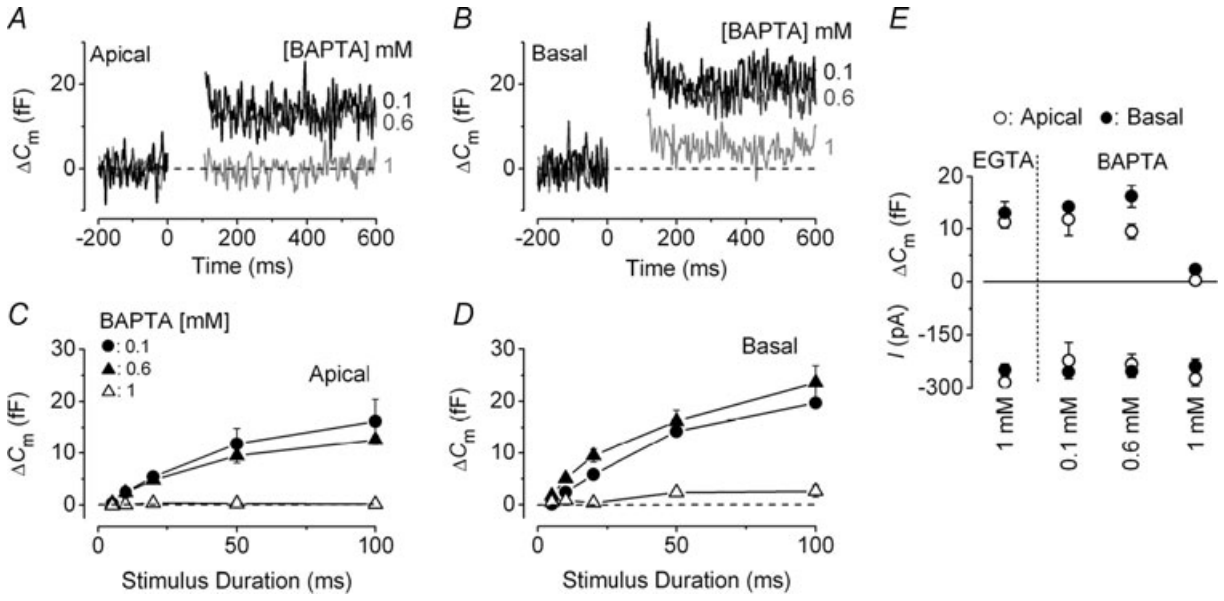

Figure 5. Coupling between Ca^{2+} channels and the RRP in immature gerbil IHCs
A and *B*, ΔC_m recordings from apical (*A*) and basal (*B*) immature IHCs in response to a 100 ms voltage step (from -81 mV to around -11 mV) using 0.1 mM, 0.6 mM and 1 mM intracellular BAPTA. *C* and *D*, average ΔC_m from apical and basal IHCs, respectively, in response to voltage steps between 5 ms and 100 ms using the above BAPTA concentrations. *E*, average ΔC_m (top panel) and peak I_{Ca} (bottom panel) at 50 ms, in order to measure the isolated RRP, from data shown in *C* and *D*. ΔC_m values obtained in EGTA from Fig. 1*C* were also included. Number of cells in EGTA (1 mM) and BAPTA (0.1, 0.6, 1 mM) are: apical: 6, 3, 3, 3 (P5–P8); basal: 10, 1, 4, 4 (P6–P8).

Discussion

In the present study we have investigated the biophysical properties of neurotransmitter release at ribbon synapses of immature mammalian hair cells using capacitance measurements. Recordings were performed using body temperature and physiological extracellular Ca^{2+}. We found that, in contrast to adult animals (Johnson *et al.* 2008), the kinetic properties of exocytosis in immature IHCs were similar between apical and basal cells. However, the developmental time course of the exocytotic Ca^{2+} dependence differed in IHCs from the two cochlear regions. We have also provided an indication of the coupling between Ca^{2+} channels and release sites in immature IHCs. Finally, ΔC_m in immature OHCs was much smaller compared to that of IHCs, consistent with there being fewer synaptic active zones in OHCs.

Neurotransmitter release at ribbon synapses of immature hair cells

Immature apical and basal gerbil IHCs showed a similar size of ΔC_m and at least two kinetic components of synaptic vesicle release could be isolated. The initial fast component (RRP: Moser & Beutner, 2000) exhibited a release time constant of about 31 ms that was comparable to adult gerbil IHCs (42–52 ms: Johnson *et al.* 2008). However, the larger number of synaptic ribbons in pre-hearing IHCs (Table 1) means that their release rate per ribbon is actually about half that of adult cells. The reduction in ribbon number with maturation is likely to be a consequence of the pruning of immature branched afferent endings to reach their characteristic unbranched configuration with adult IHCs (Pujol *et al.* 1998). The larger pool size and greater release rate of the RRP per ribbon in adult IHCs (Table 1) could promote the coincidence of release events, which seems to be required for accurate temporal coding of sound (Moser *et al.* 2006, Wittig & Parsons, 2008). The refilling of the RRP in pre-hearing IHCs is unlikely to become rate limiting for vesicle release for frequencies up to at least 7 Hz, which is in the range of the predicted frequency of spontaneous Ca^{2+} action potentials intrinsic to these cells (<10 Hz: Johnson & Marcotti, 2008). In contrast to the RRP, the SRP release rate per ribbon in immature IHCs was faster than that of adult cells (Table 1). This is unlikely to be a consequence of the larger I_{Ca} in immature IHCs because it cannot explain their comparatively lower RRP release rate. The inverse relation of the RRP and SRP release rates between immature and adult IHCs appears to be correlated with the cell's different exocytotic Ca^{2+} dependence (Fig. 4*C*), especially considering that the rates for adult apical cells lie in between (Table 1). The lower demand for maintained exocytosis in immature spiking IHCs could also explain

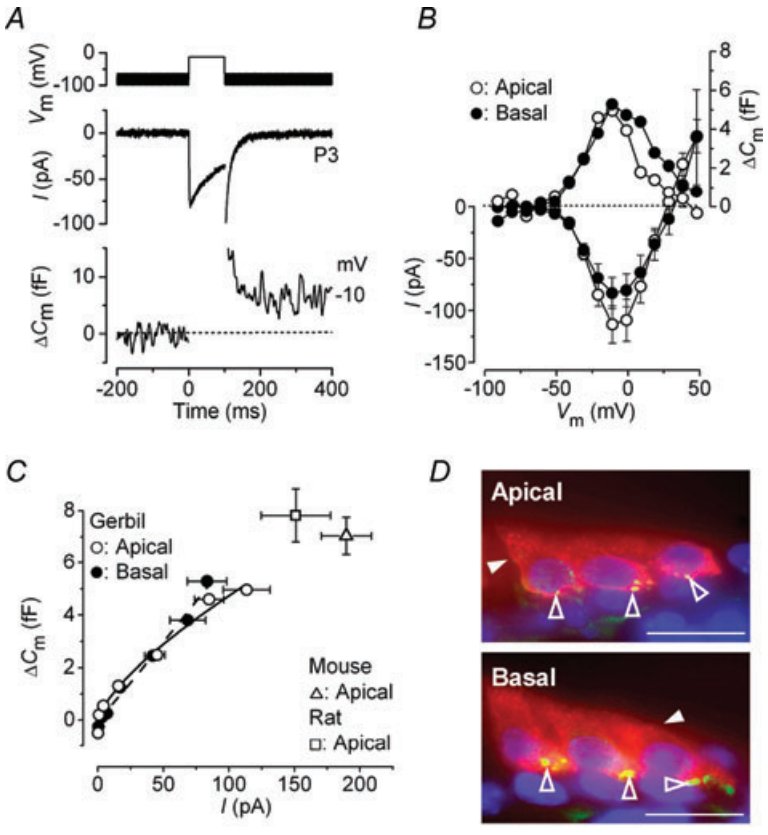

Figure 6. Neurotransmitter release in immature gerbil OHCs
A, I_{Ca} and ΔC_m responses recorded from an apical P3 gerbil OHC. Voltage protocol as described in Fig. 1*A* but using 5 mM extracellular Ca^{2+}. Traces are the average of three protocol repetitions. *B*, average peak *I–V* and ΔC_m–*V* curves from apical and basal OHCs (P3, $n = 4$ for each) using depolarizing voltage steps in 10 mV increments from −81 mV. The ΔC_m values do not have S.E.M. since they were directly measured from the averaged traces of pooled cells. *C*, synaptic transfer functions for apical and basal OHCs. Average ΔC_m was plotted against the corresponding I_{Ca}, between −71 mV and near −10 mV, from the *I–V* and ΔC_m–*V* curves shown in *B*. Fits to the data points are according to eqn (1). The open triangle and square indicate the peak responses obtained from C57B mouse ($n = 6$) and rat ($n = 6$) apical OHCs, respectively. *D*, immunolocalization of active zones (green: open arrowheads) and otoferlin (red: closed arrowheads) in apical and basal gerbil OHCs (P4). The number of active zones in OHCs was: 1st row 8.9 ± 1.1 ($n = 8$), 2nd row 8.6 ± 1.4 ($n = 8$), 3rd row 9.0 ± 1.3 ($n = 5$); in basal OHCs was: 1st row 9.3 ± 1.0 ($n = 8$), 2nd row 10.9 ± 0.7 ($n = 9$), 3rd row 11.0 ± 0.7 ($n = 8$).

the faster depletion of the SRP compared to the more sustained activity of adult cells (Table 1).

The above findings indicate that the synaptic machinery of pre-hearing IHCs lacks any position-dependent biophysical specialization that has been described in the adult gerbil cochlea (Johnson *et al.* 2008). This could indicate that in pre-hearing IHCs, possible differences in signalling characteristics such as the frequency and/or pattern of spontaneous action potentials along the gerbil cochlea (Johnson & Marcotti, 2008) do not require specialized synaptic machinery. This is in contrast to more mature IHCs where the receptor characteristics of low- and high-frequency cells are different, with basal cells responding to sound with graded receptor potentials (Russell & Sellick, 1978) while apical cells show an additional phasic component representing the sound frequency (Dallos, 1985).

Although the role of exocytosis in immature OHCs is less clear, they express $Ca_V1.3$ Ca^{2+} channels (Michna *et al.* 2003), appear to show robust exocytosis (Beurg *et al.* 2008) and have presynaptic specializations opposite to type I afferent fibres (Shnerson *et al.* 1982), which are only transiently present during early postnatal stages (Pujol *et al.* 1998). This suggests that OHCs could potentially contribute to the refinement of synaptic connections within the immature cochlea, a role only suggested for electrically active IHCs (Kros *et al.* 1998).

In the present study we have shown that early postnatal OHCs from wild-type rodents (gerbils, C57B mice and Wistar rats) exhibited relatively small exocytotic responses, which could be about an order of magnitude smaller than that of IHCs if OHCs were to be recorded under similar conditions (physiological 1.3 mM Ca^{2+}). This came as a surprise considering the large RRP size recently described in OHCs from *Otoferlin* control mice (Beurg *et al.* 2008). Moreover, *Otof* control OHCs fired spontaneous action potentials that are absent in wild-type rodents when working in near-physiological Ca^{2+} concentrations (CD-1 mice: Marcotti & Kros 1999; rats: Oliver *et al.* 1997). Together these observations suggest that the biophysical properties of OHCs in the mixed *Otof* background mouse could be somehow different to those of other wild-type animals. Moreover, the linear exocytotic Ca^{2+} dependence reported in OHCs of both mice (Beurg *et al.* 2008) and gerbils (Fig. 6*C*) is unlikely to be suitable for encoding the spiking activity (on–off events) since the release of neurotransmitter may also occur in the intervals between spikes.

Despite the relatively small ΔC_m responses of OHCs, the estimated size of the RRP at each active zone was comparable to that of immature IHCs, consisting of 15 and 13 vesicles in apical and basal cells, respectively. These numbers correlate with those obtained at IHC ribbon synapses using morphological observations ($\leq$30 vesicles per active zone in mouse: Khimich *et al.* 2005), electrophysiological recordings ($\sim$12 vesicles in rat: Goutman & Glowatzki, 2007) and also at ribbon synapses in the retina (22 vesicles: von Gersdorff *et al.* 1996). Although the release of single quanta is likely to trigger action potential activity in the afferent fibres (IHCs: Glowatzki & Fuchs, 2002), it remains unclear how immature OHCs drive afferent activity since in wild-type rodents they are not spontaneously active.

The exocytotic Ca^{2+} sensitivity at gerbil IHC synapses changes with development

The onset of hearing in most rodents occurs at around P10–P12. While immature IHCs exhibit intrinsic spontaneous Ca^{2+}-dependent action potential activity (Glowatzki & Fuchs, 2002; Marcotti *et al.* 2003), adult cells respond to sound vibration with rapid and graded receptor potentials (Russell & Sellick, 1978). It has been suggested that developmental and tonotopic differences in the exocytotic Ca^{2+} dependence are important for IHC function, allowing them to encode these different receptor potentials (mouse: Johnson *et al.* 2005; gerbil: Johnson *et al.* 2008). Our findings indicate that the transition between a high-order (immature) and a near linear (adult) relation is achieved in 2–3 days just before the onset of hearing in high-frequency cells. Although low-frequency IHCs maintain an overall higher order exocytotic Ca^{2+} dependence, its moderate decline occurred a few days later (Fig. 5: between P12 and P16), reflecting the delayed development of the apical coil (Pujol *et al.* 1998). In contrast to the Ca^{2+} dependence, the exocytotic Ca^{2+} efficiency was not fully mature until $\geq$P20, due to the size of I_{Ca} reaching a steady level at around this time. The high Ca^{2+} efficiency of exocytosis in adult IHCs is likely to drive spontaneous activity in auditory afferents, the frequency of which gradually increases only from around the onset of hearing (Woolf & Ryan, 1985). These results also suggest that some caution should be taken when investigating and comparing the biophysical properties of exocytosis at intermediate stages (P13–P18) with either immature or adult stages.

Functional Ca^{2+} coupling of gerbil IHC ribbon synapses

Although the basic biophysical development of IHC synapses is now better understood, very little information is available on the factors responsible for the developmental changes in the exocytotic Ca^{2+} dependence. It has been suggested that a close coupling between Ca^{2+} channels and release sites (creating a Ca^{2+} nanodomain) could be responsible for the linear Ca^{2+} dependence of exocytosis in adult IHCs (Brandt *et al.* 2005). Under this scenario, high Ca^{2+} cooperativity

in immature IHCs should be under the control of a Ca^{2+} microdomain. However, we found that the distance between Ca^{2+} channels and release sites in pre-hearing IHCs positioned at either end of the cochlea was in the range of 40 nm, which is comparable and even slightly closer to that found in adult cells (about 50 nm: Johnson *et al.* 2008). Therefore, exocytosis in gerbil IHCs is under a Ca^{2+} nanodomain control irrespective of age or position along the cochlea, suggesting that something other than Ca^{2+} channel localization is likely to be responsible for the modulating the Ca^{2+} sensitivity.

The different exocytotic Ca^{2+} dependence observed before and after the onset of hearing (Johnson *et al.* 2005) and as a function of tonotopic position in adult gerbils (Johnson *et al.* 2008) is likely to be intrinsic to the synaptic machinery of IHCs. Therefore, corresponding differences in the expression of Ca^{2+} sensing molecules at IHC ribbon synapses has to be considered. So far, the proposed candidate to fulfil this role in auditory but not in vestibular hair cells is otoferlin (Roux *et al.* 2006; Beurg *et al.* 2008). Since otoferlin appears to be similarly distributed in immature (Figs 1*E* and 6*D*) and adult gerbil hair cells (Johnson *et al.* 2008; for mouse see Roux *et al.* 2006), it is unlikely that it alone could control both the high-order (immature IHCs $N \approx 4$; low-frequency adult cells $N \approx 2$–3: Fig. 4*C*) and linear (high-frequency adult IHCs: Fig. 4*C*; immature OHCs: Fig. 6*C*) Ca^{2+} dependence of exocytosis in mammalian cochlear hair cells. Therefore, additional as yet unknown Ca^{2+} sensing proteins or promoters of exocytosis (Jahn *et al.* 2003), which are differentially expressed as a function of development and cochlear position, could be involved.

References

Augustine GJ, Charlton MP & Smith SJ (1985). Calcium entry and transmitter release at voltage-clamped nerve terminals of squid. *J Physiol* **367**, 163–181.

Berridge MJ, Lipp P & Bootman MD (2000). The versatility and universality of calcium signalling. *Nat Rev Mol Cell Biol* **1**, 11–21.

Beurg M, Safieddine S, Roux I, Bouleau Y, Petit C & Dulon D (2008). Calcium- and otoferlin-dependent exocytosis by immature outer hair cells. *J Neurosci* **28**, 1798–1803.

Beutner D & Moser T (2001). The presynaptic function of mouse cochlear inner hair cells during development of hearing. *J Neurosci* **21**, 4593–4599.

Brandt A, Striessnig J & Moser T (2003). $Ca_V1.3$ channels are essential for development and presynaptic activity of cochlear inner hair cells. *J Neurosci* **23**, 10832–10840.

Brandt A, Khimich D & Moser T (2005). Few $Ca_V1.3$ channels regulate the exocytosis of a synaptic vesicle at the hair cell ribbon synapse. *J Neurosci* **25**, 11577–11585.

Dallos P (1985) Response characteristics of mammalian cochlear hair cells. *J Neurosci* **5**, 1591–1608.

Dallos P (1992). The active cochlea. *J Neurosci* **12**, 4575–4585.

Fuchs PA (2005). Time and intensity coding at the hair cell's ribbon synapse. *J Physiol* **566**, 7–12.

Glowatzki E & Fuchs PA (2002). Transmitter release at the hair cell ribbon synapse. *Nat Neurosci* **5**, 147–154.

Goutman JD & Glowatzki E (2007). Time course and calcium dependence of transmitter release at a single ribbon synapse. *Proc Natl Acad Sci U S A* **104**,16341–16346.

Glowatzki E, Grant L & Fuchs PA (2008). Hair cell afferent synapses. *Curr Opin Neurobiol* **18**, 389–395.

Greenwood DD (1990). A cochlear frequency-position function for several species-29 years later. *J Acoust Soc Am* **87**, 2592–2605.

Griesinger CB, Richards CD & Ashmore JF (2005). Fast vesicle replenishment allows indefatigable signalling at the first auditory synapse. *Nature* **435**, 212–215.

Guinan JJ Jr (1996). Physiology of olivocochlear efferents. In *The Cochlea*, ed. Dallos P, Popper AN & Fay RR, pp. 435–502. Springer, New York.

Jahn R, Lang T & Südhof TC (2003). Membrane fusion. *Cell* **112**, 519–533.

Johnson SL, Marcotti W & Kros CJ (2005). Increase in efficiency and reduction in Ca^{2+} dependence of exocytosis during development of mouse inner hair cells. *J Physiol* **563**, 177–191.

Johnson SL, Adelman JP & Marcotti W (2007). Genetic deletion of SK2 channels in mouse inner hair cells prevents the developmental linearization in the Ca^{2+} dependence of exocytosis. *J Physiol* **583**, 631–646.

Johnson SL & Marcotti W (2008). Biophysical properties of $Ca_V1.3$ calcium channels in gerbil inner hair cells. *J Physiol* **586**, 1029–1042.

Johnson SL, Forge A, Knipper M, Münkner S, Marcotti W (2008). Tonotopic variation in the calcium dependence of neurotransmitter release and vesicle pool replenishment at mammalian auditory ribbon synapses. *J Neurosci* **28**, 7670–7678.

Khimich D, Nouvian R, Pujol R, tom Dieck S, Egner A, Gundelfinger ED & Moser T (2005). Hair cells synaptic ribbons are essential for synchronous auditory signalling. *Nature* **434**, 889–894.

Kros CJ, Ruppersberg JP & Rüsch A (1998). Expression of a potassium current in inner hair cells during development of hearing in mice. *Nature* **394**, 281–284.

Lenzi D, Runyeon JW, Crum J, Ellisman MK & Roberts WM (1999). Synaptic vesicle populations in saccular hair cells reconstructed by electron tomography. *J Neurosci* **19**, 119–132.

Marcotti W & Kros CJ (1999). Developmental expression of the potassium current $I_{K,n}$ contributes to maturation of mouse outer hair cells. *J Physiol* **520**, 653–660.

Marcotti W, Johnson SL, Rüsch A & Kros CJ (2003). Sodium and calcium currents shape action potentials in immature mouse inner hair cells. *J Physiol* **552**, 743–761.

Michna M, Knirsch M, Hoda JC, Muenkner S, Langer P, Platzer J, Striessnig J & Engel J (2003). Cav1.3 (α1D) Ca^{2+} currents in neonatal outer hair cells of mice. *J Physiol* **553**, 747–758.

Moser T & Beutner D (2000). Kinetics of exocytosis and endocytosis at the cochlear inner hair cell afferent synapse of the mouse. *Proc Natl Acad Sci U S A* **97**, 883–888.

Moser T, Neef A & Khimich D (2006). Mechanisms underlying the temporal precision of sound coding at the inner hair cell ribbon synapse. *J Physiol* **576**, 55–62.

Müller M (1996). The cochlear place-frequency map of the adult and developing Mongolian gerbil. *Hear Res* **94**, 148–156.

Naraghi M & Neher E (1997). Linearized buffered Ca^{2+} diffusion in microdomains and its implications for calculation of $[Ca^{2+}]$ at the mouth of a calcium channel. *J Neurosci* **17**, 6961–6973.

Neher E (1998). Vesicle pools and Ca^{2+} microdomains: new tools for understanding their roles in neurotransmitter release. *Neuron* **20**, 389–399.

Oliver D, Plinkert P, Zenner HP & Ruppersberg JP (1997). Sodium current expression during postnatal development of rat outer hair cells. *Pflugers Arch* **434**, 772–778.

Parsons TD, Lenzi D, Almers W & Roberts WM (1994). Calcium-triggered exocytosis and endocytosis in an isolated presynaptic cell: capacitance measurements in saccular hair cells. *Neuron* **13**, 875–883.

Platzer J, Engel J, Schrott-Fischer A, Stephan K, Bova S, Chen H, Zheng H & Striessnig J (2000). Congenital deafness and sinoatrial node dysfunction in mice lacking class D L-type Ca^{2+} channels. *Cell* **102**, 89–97.

Pujol R, Lavignr-Rebillard M & Lenoir M (1998). Development of sensory and neural structures in the mammalian cochlea. In *Development of the Auditory System*, ed. Rubel EW, Popper AN & Fay RR, pp. 146–192. Springer, New York.

Roberts WM, Jacobs RA & Hudspeth AJ (1990). Colocalization of ion channels involved in frequency selectivity and synaptic transmission at presynaptic active zones of hair cells. *J Neurosci* **10**, 3664–3684.

Roux I, Safieddine S, Nouvian R, Grati M, Simmler MC, Bahloul A, Perfettini I, Le Gall M, Rostaing P, Hamard G, Triller A, Avan P, Moser T & Petit C (2006). Otoferlin, defective in a human deafness form, is essential for exocytosis at the auditory ribbon synapse. *Cell* **127**, 277–289.

Russell IJ & Sellick PM (1978). Intracellular studies of hair cells in the mammalian cochlea. *J Physiol* **284**, 261–290.

Schug N, Braig C, Zimmermann U, Engel J, Winter H, Ruth P, Blin N, Pfister M, Kalbacher H & Knipper M (2006). Differential expression of otoferlin in brain, vestibular system, immature and mature cochlea of the rat. *Eur J Neurosci* **24**, 3372–3380.

Schmitz F, Königstorfer A & Südhof TC (2000). RIBEYE, a component of synaptic ribbons: a protein's journey through evolution provides insight into synaptic ribbon function. *Neuron* **28**, 857–872.

Shnerson A, Devigne C & Pujol R (1982). Age-related changes in the C57BL/6J mouse cochlea. II. Ultrastructural findings. *Dev Brain Res* **2**, 77–88.

Sobkowicz HM, Rose JE, Scott GE & Slapnick SM (1982). Ribbon synapses in the developing intact and cultured organ of Corti in the mouse. *J Neurosci* **2**, 942–957.

Spitzer NC, Lautermilch NJ, Smith RD & Gomez TM (2000). Coding of neuronal differentiation by calcium transients. *BioEssays* 22, 811–817.

Sterling P & Matthews G (2005). Structure and function of ribbon synapses. *Trends Neurosci* **28**, 20–29.

Tucker T & Fettiplace R (1995). Confocal imaging of calcium microdomains and calcium extrusion in turtle hair cells. *Neuron* **15**, 1323–1335.

von Gersdorff H, Vardi E, Matthews G & Sterling P (1996). Evidence that vesicles on the synaptic ribbon of retinal bipolar neurons can be rapidly released. *Neuron* **16**, 1221–1227.

Wittig JH & Parsons TD (2008). Synaptic ribbon enables temporal precision of hair cell afferent synapse by increasing the number of readily releasable vesicles: a modeling study. *J Neurophysiol* **100**, 1724–1739.

Woolf NK & Ryan AF (1985). Ontogeny of neural discharge patterns in the ventral cochlear nucleus of the Mongolian gerbil. *Dev Brain Res* **17**, 131–147

Author contributions

S.L.J. collected and analysed the electrophysiological data (in the UK) and helped write the paper. C.F. performed the immunolabelling experiments in Germany. M.K. supervised and analysed immunolabelling experiments. All authors contributed to the design of the research. W.M. conceived and coordinated the study, supervised the experiments, participated in data collection and analysis and wrote the paper. All authors discussed the results, commented on the manuscript and approved the version to be published.

Acknowledgements

This work was supported by Wellcome Trust, Deafness Research UK and Royal Society grants to W.M. and by a Baden-Württemberg research grant to M.K. W.M. is a Royal Society University Research Fellow. We would like to thank M. J. Palmer for her very constructive comments on an earlier version of the manuscript and M. Cardwell and A. Davids for their excellent assistance with the animals. We thank N. Blin and M. Pfister (University of Tübingen, Germany) for their generous supply of the otoferlin antibody.